Macromolecules

pubs.acs.org/Macromolecules Article

Morphology of Isotactic Polypropylene–Polyethylene Block Copolymers Driven by Controlled Crystallization

Claudio De Rosa,* Anna Malafronte, Rocco Di Girolamo, Finizia Auriemma, Miriam Scoti, Odda Ruiz de Ballesteros, and Geoffrey W. Coates

Cite This: https://dx.doi.org/10.1021/acs.macromol.0c01316 Read Online

ACCESS | Metrics & More | Article Recommendations | Supporting Information

ABSTRACT: A study of the morphology of diblock copolymers composed of two crystalline blocks of isotactic polypropylene (iPP) and polyethylene (PE) is shown. The samples form phase-separated structures in the melt because of the incompatibility between iPP and PE blocks. Cylindrical PE microdomains are visible at room temperature in the sample with a PE volume fraction of 26%, rapidly quenched from the melt in liquid nitrogen. In the quenched sample, PE crystallizes inside the PE cylindrical microdomains, whereas crystals of iPP are not visible in the iPP domains because the quenching prevents crystallization of the lamellar α form. Less rapid cooling of the melt produces, instead, breakout crystallization, where the phase-separated structure of the melt is destroyed by the slow crystallization of the α form of iPP and of PE. The succession of crystallization of iPP and PE and the resulting final morphology have been analyzed by inducing selective and different orientations of iPP and PE crystals through epitaxial crystallization onto the benzoic acid (BA) crystal substrate. Epitaxy produces oriented crystallization of iPP and PE, with a unique alignment of PE lamellar crystals and a double orientation of iPP crystals on to the (001) exposed face of BA. Epitaxy destroys the phase-separated structure of the melt and induces the formation of ordered lamellar nanostructures with alternated layers of iPP and PE, whose orientation is defined by the alignment of PE or iPP crystals, which, in turn, is determined by epitaxy. The results indicate that crystalline block copolymers offer the opportunity to create nanoscale patterns on thin films and improve the possibility of controlling the microstructure of block copolymers and the alignment of microdomains by controlling the crystallization process.

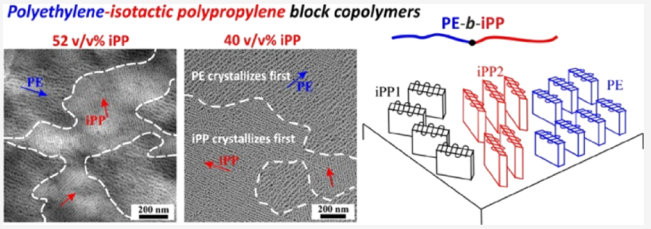

INTRODUCTION

Semicrystalline block copolymers (BCPs) combining crystallizable blocks of isotactic polypropylene (iPP) and polyethylene (PE) have recently received considerable attention thanks to the possibility to use them as compatibilizers in poorly miscible iPP/PE blends, opening new opportunities for recycling polyolefins into equal- or higher-value materials with lower sorting costs.[1−3] The preparation of iPP−PE BCPs with precise control over block length and architecture offers the possibility to tailor the final properties of the material, thus further expanding the already enormous range of applications of iPP and PE homopolymers in packaging, textile, and cutting edge automotive and aircraft markets.[4,5] Despite the tremendous applicative potential of these materials, the synthesis of iPP−PE BCPs[6] has been very challenging because of the difficulties concerning the evolution of living polymerization methods[7,8] that guarantee obtaining high-molecular mass polymers with a high control of the stereochemistry and high level of stereoregularity. Semicrystalline iPP−PE BCPs with a high molecular mass and with precise control over block length and architecture have been recently obtained by using a pyridylamidohafnium precatalyst activated with $B(C_6F_5)_3$,[1,2,9] which follows the extensive effort in obtaining living iPP with this class of catalysts.[10−12] The obtained materials, consisting of semicrystalline stereoregular iPP and linear PE blocks, display superior interfacial activity, effectively compatibilizing PE/iPP blends and dramatically improving the tensile properties of blends for certain combinations of block molecular masses and molecular architectures.[1,2] An in depth study of the morphology and crystallization behavior of these new double crystalline BCPs (CC-BCPs) is still lacking.

Crystallization in BCPs has attracted much attention, and several reviews have been published on the topic.[13−16] The ability of BCPs to self-assemble because of the relative repulsion between its components is well known.[17,18] The resulting formation of nanostructures with periodicity in the nanoscale has attracted increasing interest for many applications, in particular as a mean for patterning solid surfaces.[19−25] However, controlling the self-assembly process

Received: June 5, 2020
Revised: October 12, 2020

Table 1. Number Average Molecular Mass (M_n), Polydispersity ($Đ = M_w/M_n$), Weight (w_{iPP}) and Volume (f_{iPP}) Fraction of the iPP Block, Number Average Molecular Mass of iPP ($M_{n(iPP)}$) and PE ($M_{n(PE)}$) Blocks, Melting Temperature (T_m) of the iPP Homopolymer and iPP–PE BCPs, and Periodicities (L) of the Nanostructures Observed in the BCP Samples Epitaxially Crystallized onto BA

sample	M_n[a] (kDa)	$Đ$[a]	w_{iPP}[b] (wt %)	f_{iPP}[c] (v/v %)	$M_{n(iPP)}$[a] (kDa)	$M_{n(PE)}$[d] (kDa)	T_m[e] (°C)	L_{iPP}[g] (nm)	L_{PE}[g] (nm)
iPP	139.8	1.29	100	100	139.8		134	35 ± 4	
iPP–PE-74	140.1	1.23	74	74	103.4	36.7	129 (135)[f]	20 ± 2	33 ± 4
iPP–PE-52	180.6	1.26	64	52	94.6	86.0	130 (135)[f]	14 ± 1	23 ± 2
iPP–PE-40	163.5	1.19	52	40	64.6	98.9	132	16 ± 2	28 ± 2

[a]From GPC. [b]Evaluated from ^{13}C NMR spectra. [c]Determined from the molecular masses $M_{n(iPP)}$ and $M_{n(PE)}$, by using the densities of amorphous iPP (0.850 g/cm^3) and PE (0.853 g/cm^3), as $f_{iPP} = (M_{n(iPP)}/0.850)/(M_{n(iPP)}/0.850 + M_{n(PE)}/0.853)$. [d]Determined from the total molecular mass M_n and the molecular mass of the iPP block as $M_{n(PE)} = M_n - M_{n(iPP)}$. [e]Evaluated from DSC heating scan at 10 °C/min of the samples crystallized by cooling the melt at 10 °C/min. [f]Shoulders of the main peak are indicated in brackets. [g]From the electron microscopy images of Figure 2 as the separation between the parallel adjacent dark lines of gold particles.

and the alignment of the nanodomains to obtain ordered patterns is still a challenge.[22]

When the BCP components can crystallize, the competition between phase separation and crystallization can create many different morphologies,[14−16] which are dependent on the values of the phase separation transition temperature of the BCP, the glass transition temperature of the amorphous block, and the crystallization temperature of the crystallizable blocks.[26,27] According to these parameters, different modes of crystallization of BCP have been described,[26] resulting in a crystallization confined within the microdomains preformed in the melt, or breaking out of the microphase-separated structure, or templated crystallization.[26]

Moreover, semicrystalline BCPs have been shown to provide new means to create nanoscale patterns on thin films.[28] Indeed, the possibility of controlling the crystallization by driving polymorphism and inducing alignment of crystalline chains within block domains is an opportunity to improve controlling the final BCP structure and the alignment of microdomains. Epitaxial crystallization of the crystallizable blocks of BCPs on the surface of low molecular mass crystalline substances has shown great potential for inducing the orientation of crystalline domains and, as a consequence, of the BCP nanodomains.[28−35]

In this paper, we report the characterization of the microstructure of crystalline–crystalline diblock copolymers (CC-BCP) constituted by blocks of iPP and PE (iPP–PE) of different molecular masses. The succession of crystallization of iPP and PE and the resulting final morphology have been analyzed by inducing selective and different alignments of the crystals of iPP and PE through epitaxial crystallization onto crystals of benzoic acid (BA).

Epitaxial crystallization is a well-established method used for semicrystalline homopolymers to induce preferred orientation of crystals on a substrate and/or to drive crystallization of a particular polymorph.[36−41] In particular, epitaxial crystallization of PE and iPP homopolymers onto BA is well known and has been well explained in terms of matching between crystalline periodicities of polymers and substrates.[39−41] Moreover, the epitaxial crystallization of PE blocks of crystalline–amorphous BCPs,[28−31,34,35] or of double crystalline block copolymers with a PE block linked to a syndiotactic polypropylene block, have also been reported.[33,35] In addition, heteroepitaxy involving PE and iPP homopolymers has been also investigated.[42−45]

Here, we report a study of the epitaxial crystallization onto BA of samples in which the iPP and PE polymers are covalently linked together to form high molecular mass CC-BCPs. The phase separation, crystallization, and morphology relationships of the CC-BCPs have been investigated. This study shows that crystallization in BCP offers the unique opportunity to control the microstructure of the nanostructure by choosing the appropriate crystallization conditions.

EXPERIMENTAL SECTION

The iPP homopolymer and iPP–PE CC-BCPs were synthesized by living and stereospecific polymerization, as described in ref 1, by using an isoselective pyridylamidohafnium catalyst activated with $B(C_6F_5)_3$. Samples with different lengths of iPP and PE blocks were prepared, with the volume fraction of the iPP block variable from 40 to 75% (Table 1). The samples, as listed in Table 1, are identified with the code iPP–PE-x, where x is the volume fraction of the iPP block.

Films with thickness lower than 40 nm of iPP and iPP–PE samples were prepared by casting from p-xylene solutions (0.5 wt %) at a temperature of ≈40 °C.

Epitaxial crystallizations were performed using as substrate crystals of BA (melting temperature equal to 123 °C), following procedures described in the literature.[39] In particular, the iPP and iPP–PE films, prepared onto microscope glass slides, were melted along with BA at temperatures above the melting temperatures of the BCP samples (Table 1), and then the mixtures were crystallized by moving the glass slide slowly down the temperature gradient of a hot bar (cooling rate 10–15 °C/min). On cooling, the BA substrate crystals grow first and after the polymer crystallizes epitaxially on the BA crystals. The substrate crystals were subsequently dissolved in hot ethyl alcohol, and the polymer film left on the glass. The thus obtained thin films crystallized onto BA were carbon coated under vacuum in an EMITECH K950X evaporator, analyzed by transmission electron microscopy (TEM) in bright field (BF) and dark field (DF) modes and electron diffraction (ED).

BCP samples were also crystallized in the absence of BA by slow cooling or fast quenching the melt into liquid nitrogen. The slowly crystallized samples were obtained by melting the iPP–PE thin films, prepared by casting onto microscope glass slides, at ≈220 °C for 5 min and then cooled by moving the slides slowly down the temperature gradient of the hot bar (cooling rate 10–15 °C/min). The films were then transferred onto TEM grids and analyzed by TEM. Thin films for the quenched samples were, instead, prepared by casting directly onto carbon-coated copper TEM grids. The films were then melted at ≈220 °C for 5 min and then quickly cooled by quenching in liquid nitrogen.

Some specimens for TEM observation were exposed to RuO_4 vapors at 25 °C for 2.5–5 h to stain the amorphous phases in PE and iPP microdomains. To improve contrast, some films crystallized onto BA were decorated with gold nanoparticles using the method of vacuum evaporation and condensation.[46,47] After evaporation, gold condensates and deposits mainly at the amorphous–crystalline interface of the semicrystalline lamellae, allowing better visualization of crystalline phases.[47,48]

https://dx.doi.org/10.1021/acs.macromol.0c01316
Macromolecules XXXX, XXX, XXX–XXX

TEM images and selected-area ED patterns (EDPs) were acquired by using a FEI TECNAI G^2 200 kV S-TWIN microscope (electron source with LaB_6 emitter). BF TEM images were acquired at 120 or 200 kV by using a spot size equal to 3, integration time 1 s, and binning 1. The selected-area (aperture of diameter of 50 μm) EDPs were acquired at 120 or 200 kV by using spot size 5−6, integration time 1−3 s, and binning 1−4. A camera length equal to 0.970 m was used to acquire the EDPs of the iPP and iPP−PE-74 samples. A 0.680 m camera length was, instead, used for the sample iPP−PE-40. DF images were obtained using a single diffraction spot of PE, the 020 reflection to image the PE crystalline lamellae.

The periodicities of the nanostructures (L) were determined by measuring the separation between the parallel adjacent dark lines of gold particles in the TEM images, using ImageJ software (National Institutes of Health, available free of charge at Web site https://imagej.nih.gov/ij/). At least 100 independent measurements were taken at different locations of the TEM images of the samples. The measurements were also confirmed by repeating the analysis on images of independent samples.

RESULTS AND DISCUSSION

Samples of iPP homopolymer and iPP−PE BCPs having different molecular masses of PE and iPP blocks and volume fractions of the iPP block variable from 40 to 75% have been prepared.[1] The samples have a similar total molecular mass with M_n spreading in the range 140−181 kDa (Table 1) and differ in the relative molecular weights of the two blocks. A symmetric BCP with PE and iPP blocks of similar lengths (sample iPP−PE-52, with $M_{n\ (iPP\ or\ PE)} \approx 90{,}000$ Da) is compared with asymmetric samples iPP−PE-74, characterized by the iPP block longer than the PE block ($M_{n(iPP)}$ = 103,400 Da, $M_{n(PE)}$ = 36,700 Da) and iPP−PE-40 with the block of PE longer than iPP ($M_{n(iPP)}$ = 64,600 Da, $M_{n(PE)}$ = 98,900 Da).

The iPP homopolymer, prepared in the same polymerization condition as the BCPs, crystallizes mainly in the α form of iPP with melting temperature of 134 °C (Table 1). This rather low melting temperature is related to a moderate level of isotacticity produced by the pyridylamidohafnium catalyst,[1,2] and the inclusion of stereo- and regiodefects,[1] with the amount of the isotactic pentad *mmmm* of 91%, as evaluated by ^{13}C NMR.[1] Accordingly, the iPP sample crystallizes by cooling the melt in a mixture of α and γ forms. The blocks of iPP in the iPP−PE samples show the same isotacticity and crystallize in mixtures of α and γ forms with a similar melting temperature (Table 1).[1,2] The block of PE crystallizes in all iPP−PE samples in the usual stable orthorhombic form of PE and show a melting temperature of 134−135 °C (Table 1), close to that of the iPP block.[1,2]

Because PE and iPP components are incompatible and tend to give phase separation,[1,2] it is expected that iPP−PE BCPs form a phase-separated microstructure in the melt and in the amorphous phase. The morphology that develops in these iPP−PE samples at 25 °C upon crystallization from the heterogeneous melt has been detected by TEM in BF mode of iPP−PE samples crystallized at different cooling rates from the melt. Films (40 nm thick) were obtained by casting from *p*-xylene solutions on glass slides, melted at ≈220 °C for 5 min and then slowly crystallized by cooling to 25 °C or rapidly crystallized by fast quenching in liquid nitrogen. The fast quenching should freeze the structure formed in the melt and allow imaging the phase-separated structure at 25 °C even after crystallization.

The BF-TEM images of iPP−PE-74 with the volume fraction of the iPP block of 74% melt-crystallized by slow cooling (cooling rate 10−15 °C/min) and fast quenching and stained with RuO_4 are shown in Figure 1A,B, respectively. In both images, the dark regions are the stained amorphous phase, whereas the light regions correspond to crystalline PE or iPP undistinguishable lamellae.

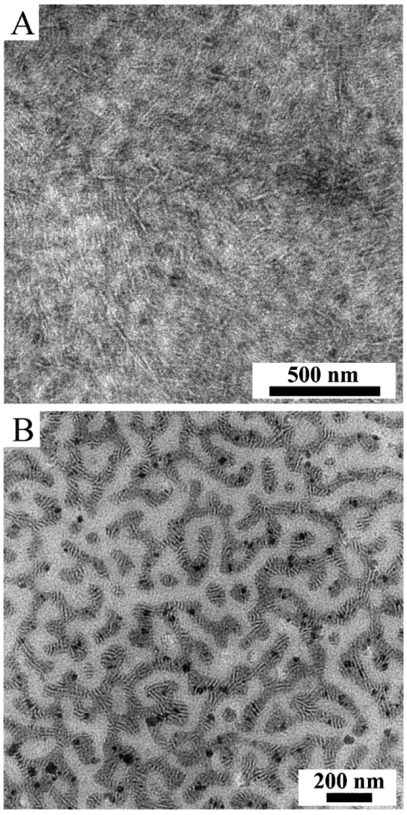

Figure 1. BF-TEM images of the sample iPP−PE-74 with a 74% volume fraction of iPP component melt-crystallized by slow cooling to 25 °C at 10−15 °C/min (A) and by fast quenching in liquid nitrogen (B) and stained with RuO_4.

Figure 1 clearly shows that the morphologies obtained in the two different crystallization conditions are completely different. For the slowly crystallized sample (Figure 1A), thin crystalline lamellae randomly oriented and homogeneously distributed over the whole sample are visible. Lamellae of iPP and PE are clearly not distinguishable and the phase-separated structure eventually existing in the melt is not visible, probably destroyed by the successive slow crystallization. This is a classic example of breakout crystallization,[26,35] where the segregation and crystallization strengths are such that the crystallization is not confined within preformed microdomains but produces randomly oriented lamellae that destroy the melt structure.

When the same sample is rapidly melt-crystallized by quenching, the phase-separated structure probably existing in the melt is visible at room temperature (Figure 1B). The darker microdomains correspond to PE domains of width of nearly 60 nm, probably cylinders as suggested by a PE volume fraction of 26%, and the lighter domains are the iPP matrix (Figure 1B). Inside the PE cylindrical domains, thin white strips are visible that may correspond to PE lamellae crystallized inside the preformed PE microdomains (Figure 1B). In the iPP domains crystals of iPP are instead not visible, probably because the quenching prevents crystallization of the lamellar α form but produces the formation of very small crystals of the mesomorphic form of iPP with a nonlamellar

https://dx.doi.org/10.1021/acs.macromol.0c01316
Macromolecules XXXX, XXX, XXX−XXX

nodular morphology,[49−52] difficult to image at the TEM. Therefore, the cylindrical nanostructure formed in the melt is frozen at room temperature by fast quenching probably because iPP does not crystallize in the lamellar α form but crystallizes in the disordered mesomorphic form that does not disturb the initial morphology.

The iPP homopolymer and iPP−PE BCPs (films of 30−50 nm thick) have been epitaxially crystallized onto the surface of BA crystals. Some thin films were coated with gold nanoparticles before TEM analysis. Coating with gold improves contrast in the microscopy observation and allows revealing detailed aspects of the morphology. The technique of gold decoration is largely used to image lamellae of polymers in BF-TEM and obtain a reliable value of the lamellar periodicity.[46−48] The gold particles, in fact, after evaporation and condensation under vacuum, deposit on the amorphous regions at the boundary with the crystalline lamellae, enhancing the visualization of brighter crystalline lamellae.[46−48]

BF-TEM images of the iPP homopolymer and of iPP−PE BCPs epitaxially crystallized onto BA and coated with gold nanoparticles are shown in Figure 2. In all images, the black

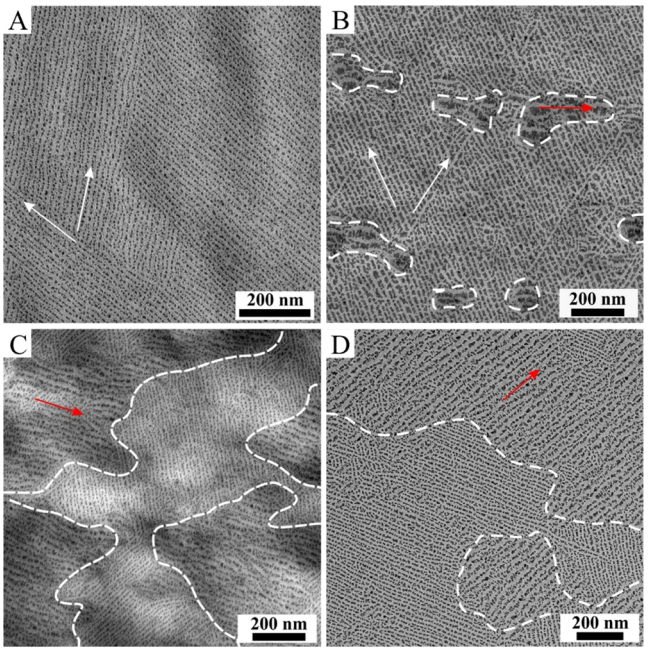

Figure 2. BF-TEM images of gold-decorated films of iPP homopolymer (A) and of iPP−PE-74 (B), iPP−PE-52 (C) and iPP−PE-40 (D) BCPs epitaxially crystallized onto BA crystals. White arrows in (A,B) show the two different directions of alignment of the two families of the iPP lamellae, whereas the red arrows in (B,C) indicate the unique direction of the alignment of PE lamellae. The dashed lines delimit the regions with a single lamellae (PE) orientation.

stains are the gold nanoparticles that are located into the amorphous phase at the interfaces with crystalline lamellae and the brighter regions correspond to iPP and/or PE crystalline lamellae (Figure 2). The selected-area EDPs of the same films of the iPP homopolymer and iPP−PE BCPs epitaxially crystallized onto BA are shown in Figure 3. The images of Figure 2 and the ED data of Figure 3 reveal the orientation of iPP and PE crystals onto the BA surface and can be explained on the basis of the epitaxy of iPP and PE onto BA crystals, deeply described in the literature for both homopolymers.[39−41]

Schemes of the relative orientations of iPP and PE crystals onto the (001) face of BA crystals described for the two homopolymers are shown in Figure 4A,B, respectively.[39−41] The crystal structure of BA is characterized by a monoclinic unit cell with parameters a = 5.510 Å, b = 5.157 Å, c = 21.973 Å, β = 97.41°, and space group $P2_1/c$.[53] Epitaxy of PE onto BA crystals is related to the crystallographic similarity between the PE interchain distance (the b-axis of PE equal to 4.93 Å)[54] and the b-axis periodicity of the BA crystal (5.157 Å),[39] and between the c-axis periodicity of PE (2.53 Å)[54] and the a-axis of BA (5.510 Å).[39] This produces the crystallization of PE on to the $(001)_{BA}$ exposed face of BA with PE lamellae standing edge-on, that is, perpendicular to the $(001)_{BA}$ plane of the BA crystal, and oriented as shown in the scheme of Figure 4B, with the PE chain axis (c_{PE}) aligned parallel to the a-axis of BA (a_{BA}), and the b-axis of PE (b_{PE}) aligned parallel to the b-axis of BA (b_{BA}).[39] The $(100)_{PE}$ lattice plane of PE is in touch with the $(001)_{BA}$ exposed face of BA. The epitaxial relationships between BA and PE are, therefore, $(100)_{PE}//(001)_{BA}$, $b_{PE}//b_{BA}$, and $c_{PE}//a_{BA}$.[39]

Epitaxy of iPP onto BA is more complex[40,41] and is strictly related to the periodicities arising in the $(010)_{iPP}$ crystallographic planes (the ac faces) of the monoclinic unit cell of the α form of iPP,[55,56] as shown in the scheme of Figure 4A.[40,41] In particular, epitaxy is due to the similarity of the iPP periodicity of 5.07 Å perpendicular to the short diagonal of the $(010)_{iPP}$ faces, which corresponds to the spacing of the $(\bar{1}01)$ planes in the α form of iPP, and the b axis periodicity of 5.16 Å of BA (Figure 4A).[40] Correspondingly, iPP crystallizes onto BA in such a way that the b axis of BA is perpendicular to the $(\bar{1}01)$ plane of the α form iPP directed along the spacing $d(\bar{1}01)$ of the $(\bar{1}01)$ planes (Figure 4A), and the a axis of BA is aligned along the short diagonal of the ac face (the $(\bar{1}01)$ plane) of iPP, that is, the [101] direction. The c axis of iPP may be aligned parallel to both the two edges of the ac face ($c_{1(iPP)}$ and $c_{2(iPP)}$ in Figure 4A).[40] Therefore, epitaxy generates two families of iPP lamellae aligned with their c axes along the two edges of the $(010)_{iPP}$ plane, more precisely along two directions tilted 50° away from the short diagonal of the ac plane (the [101] direction) and from the a axis of BA. These two families of iPP lamellae are consequently 80° apart (180° - (2 × 50°)) and inclined by about ±50° to the a axis of BA (Figure 4A).[40,41] The epitaxial relationships between BA and iPP are, therefore, $(010)_{iPP}//(001)_{BA}$, $a_{BA}//[101]_{iPP}$, and $b_{BA} \approx d(\bar{1}01)_{iPP}$.

It is to be noted that this orientation of two iPP lamellae along the two possible directions tilted away from the [101] direction is similar and corresponds to that involved in the homoepitaxy of iPP lamellae that leads to lamellar branching typical of the α form with the a and c axes of the daughter lamella aligned parallel to the c and a axes, respectively, of the mother lamella,[57,58] with the resulting formation of iPP quadrites.[59] This same orientation exists as a crystallographic feature in the γ form of iPP.[60−62]

Finally, as mentioned in the introduction, heteroepitaxy of PE and iPP crystals is also possible.[42−45] Also in this case, the $(010)_{iPP}$ plane of iPP is involved in the epitaxy, the $(100)_{PE}$ plane of PE and the $(010)_{iPP}$ plane of iPP being the contact planes.[42−45] The b axis of α form crystals of iPP (b_{ipp}) and the a axis of PE (a_{PE}) are perpendicular to the touch plane, and the chain axis of PE is aligned along the [101] direction of iPP in

https://dx.doi.org/10.1021/acs.macromol.0c01316
Macromolecules XXXX, XXX, XXX−XXX

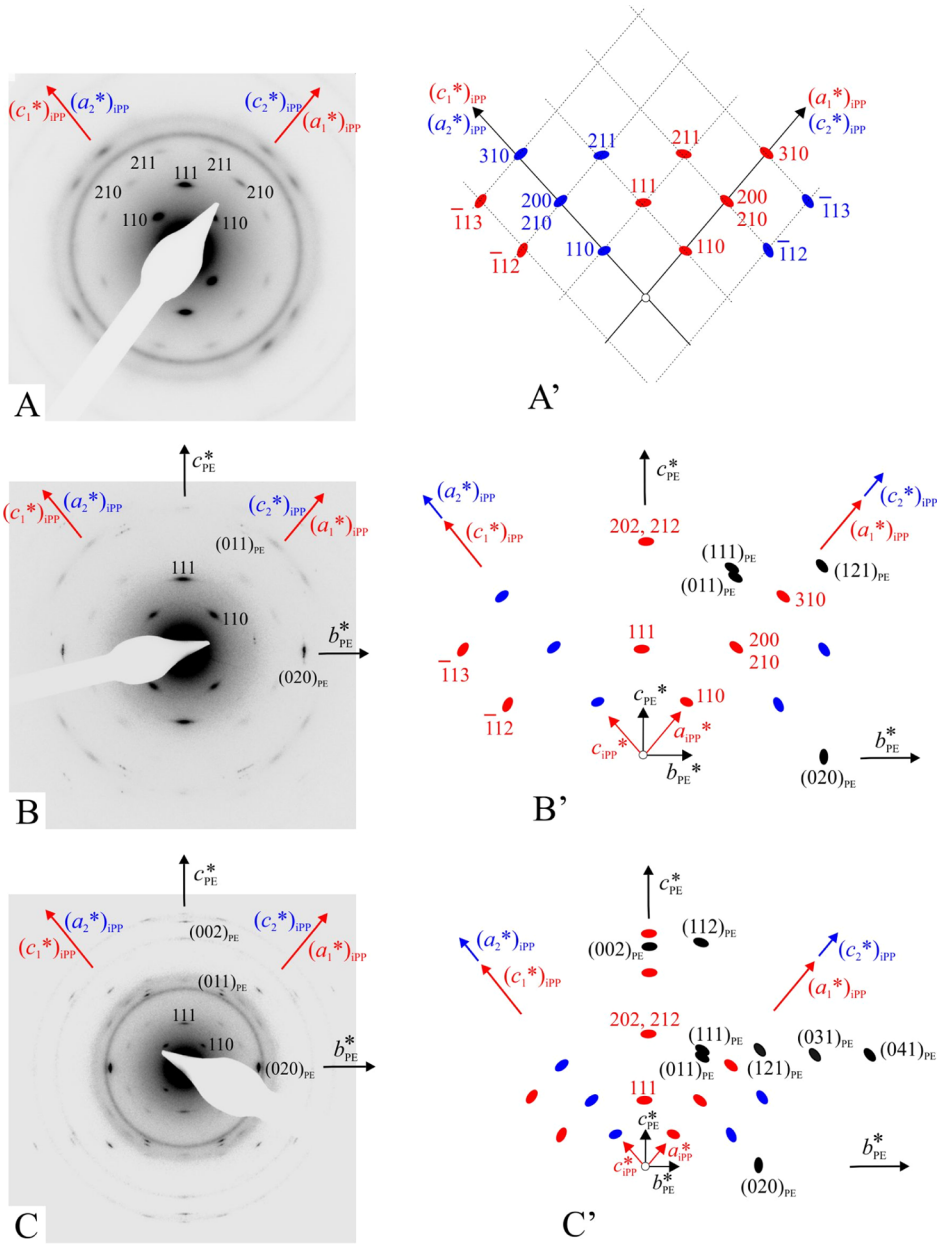

Figure 3. Selected-area EDP of films of the iPP homopolymer (A) and iPP−PE-74 (B) and iPP−PE-40 (C) BCPs epitaxially crystallized onto BA and gold decorated. Corresponding sketches of the observed reflections are represented in parts A′, B′, and C′, respectively. The *hkl* indices of the more intense observed reflections of the α form of iPP and of the orthorhombic form of PE are indicated. The orientations of the reciprocal axes b_{PE}^* and c_{PE}^* of PE and of the two families of iPP lamellae $(a_1^*)_{iPP}$, $(c_1^*)_{iPP}$ and $(a_2^*)_{iPP}$, $(c_2^*)_{iPP}$ are also indicated. In A′, the a^*c^* section of the reciprocal lattice of iPP is also drawn. The EDPs A-C were acquired in areas of the samples having morphologies represented in Figure 2A,B,D, respectively. In the sketch A′ of the EDP of the iPP homopolymer, the red and blue spots and corresponding *hkl* indices are the two different sets of reflections (mainly *h*0*l* or *h*1*l* reflections) generated by the two different families of lamellae aligned as defined by the two reciprocal lattices $(a_1^*)_{iPP}$, $(c_1^*)_{iPP}$ (in red) and $(a_2^*)_{iPP}$, $(c_2^*)_{iPP}$ (in blue). In the schemes B′ and C′ of the EDPs of the BCP samples, the red and blue spots are the reflections of the two families of iPP crystals, and the black spots correspond to the reflections generated by PE crystals oriented as defined by the reciprocal lattice a_{PE}^*, b_{PE}^*. The EDP of the sample iPP−PE-40 (C) was acquired by using a different camera length to detect additional PE and iPP reflections. The ring reflection in patterns A and C corresponds to the 111 reflection of gold used in the decoration of the films.

the α form (the short diagonal of the *ac* face), as shown in the scheme of Figure 4C.[42−45] Therefore, the chain axis of PE c_{PE} is tilted to about 50° to the chain axis of iPP c_{iPP} (Figure 4C).[45]

In the TEM image of Figure 2A, the iPP homopolymer epitaxially crystallized onto BA, the dark gold is located in the intralamellar amorphous phases, that is, in between the crystalline lamellae of iPP that appear bright. The TEM image of Figure 2A confirms the presence of two families of edge-on iPP crystalline lamellae, generated by epitaxy, highly aligned along two directions ≈60−70° apart with their chain axes *c* ($c_{1(iPP)}$ and $c_{2(iPP)}$ in Figure 4A) inclined by about ±50° to the *a* axis of BA, which is parallel to the [101] crystallographic direction of the α form of iPP (Figure 4A).[40,41] The periodicity of the lamellar structure, that is, the sum of the thicknesses of crystalline and amorphous layers, has been easily evaluated by measuring the separation between the parallel adjacent dark lines of gold particles. For both families

https://dx.doi.org/10.1021/acs.macromol.0c01316
Macromolecules XXXX, XXX, XXX−XXX

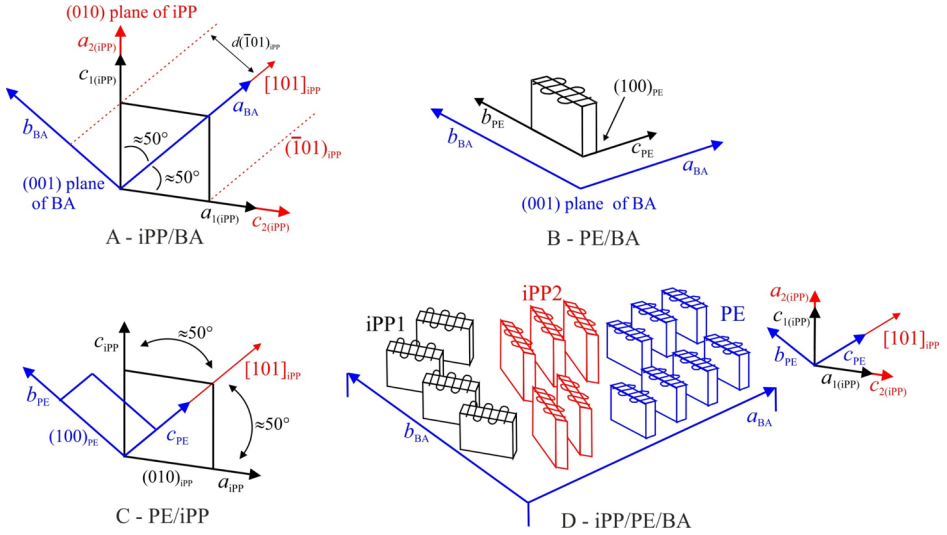

Figure 4. Schematic diagrams showing how crystals of α form of iPP (A) and PE (B) are oriented onto the $(001)_{BA}$ exposed face of BA crystals after epitaxial crystallization. (C) Scheme of the relative orientation of iPP and PE resulting from the heteroepitaxial crystallization of PE onto iPP and (D) scheme of the alignment of PE and iPP lamellae epitaxially crystallized onto BA crystals in iPP−PE BCPs. In D, PE lamellae (blue) are aligned with the c_{PE} axis parallel to the a_{BA} axis of BA and parallel to the $[101]_{iPP}$ direction of iPP, and the two families of iPP lamellae (black and red) are aligned with the two chain axes $c_{1(iPP)}$ and $c_{2(iPP)}$ directed parallel to two directions ≈60−70° apart and inclined to about 50° to the c_{PE} axis of PE (and to the a_{BA} axis of BA). The axes orientation of iPP, PE, and BA crystals are indicated. According to relative epitaxies the relationships among crystallographic parameters are: $(010)_{iPP}//(001)_{BA}//(100)_{PE}$, $c_{PE}//a_{BA}//[101]_{iPP}$, and $b_{PE}//b_{BA}$.

of iPP lamellae, a periodicity of ≈35 nm has been obtained (Table 1).

In the cases of the iPP−PE BCPs, the BF-TEM images show more complex morphologies (Figure 2B−D), compared to the iPP homopolymer, resulting from the reciprocal influence of all three involved components (iPP, PE, and BA). Straight and parallel rows of dark spots, corresponding to gold are also observed. Gold is included in the amorphous layers that represent the amorphous phases in PE and iPP domains (Figure 2B−D). Amorphous layers alternate with bright layers that coincide with iPP or PE lamellae. The BF-TEM images of the BCPs of Figure 2B−D show large regions where the bright crystalline lamellae are aligned along two directions and regions (delimited by the dashed lines) where the crystalline lamellae are aligned along one direction. Lamellae with a single orientation seem to be thicker than those with double orientations.

Figure 2B clearly shows that in the regions with a double orientation, the lamellae are aligned along two directions ≈60° apart, similar to the morphology seen in Figure 2A for the iPP homopolymer. This suggests that the thinner crystalline lamellae with a double orientation are the iPP lamellae. Considering that the epitaxy of PE onto BA produces the alignment of the PE lamellae along one direction, as shown in Figure 4B, in the BF-TEM images of Figure 2B−D of the BCPs the thicker crystalline lamellae aligned along one direction are the PE lamellae. This is confirmed by the observation that the regions containing lamellae with a unique orientation (delimited by the dashed lines) become larger with increasing the length and the volume fraction of the PE block. These regions are, indeed, very small for iPP−PE-74 with 74 v/v % of iPP, as shown in Figure 2B, but are much larger for iPP−PE-40 with 40 v/v % of iPP, as shown in Figure 2D.

The periodicity of the lamellar nanostructures in the BCPs has also been estimated as the separation of the parallel adjacent dark lines of gold in the BF-TEM images of Figures 2B−D. For the iPP lamellae (in the regions with double orientation), values of periodicity comprised between 14 and 20 nm were measured (Table 1), less than the value of 35 nm obtained for the iPP homopolymer (Figure 2A). For the PE lamellae (in the regions of Figure 2B−D with single orientation), values of periodicity between 23 and 33 nm were estimated (Table 1).

It is worth noting that the BF-TEM images of Figure 1A of the sample iPP−PE-74 and of Figure S1 (see Supporting Information) of the sample iPP−PE-40 crystallized without BA, stained with RuO_4 or gold decorated, show a random orientation of undistinguishable PE and iPP lamellae. Therefore, the images of Figure 2 clearly demonstrate that the epitaxial crystallization allows to distinguish the iPP and PE crystalline lamellae on the basis of the different induced orientations.

The alignment of iPP and PE crystalline lamellae has been confirmed by ED. The selected-area EDPs of films of the iPP homopolymer and iPP−PE-74 and iPP−PE-40 BCPs epitaxially crystallized onto BA are represented in Figure 3A,B,C, respectively. The EDPs are acquired in regions of the samples having morphologies similar to those represented in Figure 2A,B,D. In particular, for the iPP homopolymer (Figure 3A) and iPP−PE-40 (Figure 3C) samples, the EDPs are acquired from the gold-decorated specimens, as shown in Figure 2A,D, respectively. For the sample iPP−PE-74, the EDP of Figure 3B has been recorded from a thin film as that of Figure 2B but stained with RuO_4. The EDPs (Figure 3A−C) contain reflections of iPP in its α form[55,56,63] and PE in its stable orthorhombic form.[54] A sketch of the patterns showing the indices *hkl* of the main observed reflections and corresponding reciprocal lattices are represented in Figure 3A′−C′. The Bragg distances of all observed *hkl* reflections (d_o) are listed in Table S1 of Supporting Information.

The sharp spots present in the EDPs indicates the crystallization of PE and iPP with high orientation of crystals (single-crystal like) defined by epitaxy onto BA. The EDP of Figure 3A of the iPP homopolymer crystallized onto BA is

https://dx.doi.org/10.1021/acs.macromol.0c01316
Macromolecules XXXX, XXX, XXX−XXX

basically the same as that of the literature[40] and is equal to those of quadrites of iPP seen along the common *b*-axis.[57] The pattern is composed of two diffraction patterns corresponding to a^*c^* sections of two reciprocal lattices of the α form of iPP, rotated each other by an angle close to the β angle of the monoclinic unit cell of the α form (Figure 3A).[40] If the a^*c^* section is in diffraction, the EDP should represent the $h0l$ section of the reciprocal lattice. The six innermost reflections having the highest intensity correspond, instead, to the 110 and 111 reflections (Figure 3A′ and Table S1) that should not be visible ($h1l$ type reflections). However, since these reflections are very strong and located near the $h0l$ plane, they appear in the EDP of Figure 3A, as also seen in the literature data,[40] because of the possible tilting of the lamellae. The EDP of Figure 3A confirms that iPP epitaxially crystallizes onto BA generating two families of lamellae of the α form oriented edge-on onto BA with the $(010)_{iPP}$ plane of the α form in touch with the $(001)_{BA}$ face of BA (Figure 4A), according to epitaxial relationships between BA and iPP

$$(010)_{iPP}//(001)_{BA},\ a_{BA}//[101]_{iPP} \text{ and } b_{BA} \approx d(\bar{1}01)_{iPP}$$

The two families of iPP lamellae are aligned with the [101] direction, the short diagonal of the *ac* face [the $(010)_{iPP}$ contact plane], parallel to the *a* axis of the BA crystal, and with the chain axes *c* of the two iPP lamellae aligned parallel to the two edges of the $(010)_{iPP}$ plane, in other words parallel to two directions tilted 50° away from the *a* axis of BA (from the [101] direction of α form of iPP) (Figure 4A). The two families of iPP lamellae result consequently being oriented 80° apart (180° - (2 × 50°)).[40,41]

The EDPs of BCP samples iPP−PE-74 and iPP−PE-40 epitaxially crystallized on BA are shown in Figure 3B,C, respectively. A similar pattern was obtained for the sample iPP−PE-52. The EDPs of the BCPs feature two families of iPP reflections (Figure 3B,B′ and C,C′), as for the iPP homopolymer (Figure 3A,A′), indicating that the covalently linked PE blocks do not influence the epitaxial crystallization of the iPP blocks of the BCPs onto the BA substrate, whatever the molecular masses of the iPP and PE blocks, and two families of iPP lamellae oriented as in Figure 4A are generated also for the BCPs. The 211 reflection seen in the EDP of the iPP homopolymer (Figure 3A,A′), due to tilting of lamellae, is not present in both EDPs of the BCP (Figure 3B,C) probably because the iPP lamellae in the BCPs are less tilted.

Besides the iPP reflections, the EDPs of Figure 3B,C also present PE reflections, in particular only reflections with $0kl$ indices, therefore, indicating that the patterns represent the b^*c^* section of the reciprocal lattice of PE (Figure 3B′,C′). The fact that the b^*c^* section is in diffraction indicates a single high alignment of the PE lamellae, positioned edge-on on the BA crystals and oriented with the chain axis *c* of PE flat on the BA surface and aligned parallel to the *a* axis of BA crystals and the *b* axis of PE parallel to the *b* axis of BA, the $(100)_{PE}$ plane of PE being in touch with the $(001)_{BA}$ exposed face of BA, as in the scheme of Figure 4B, according to the epitaxial relationships between BA and PE[39]

$$(100)_{PE}//(001)_{BA},\ b_{PE}//b_{BA} \text{ and } c_{PE}//a_{BA}$$

This orientation is equal to that reported for the PE homopolymer[39] and PE-based crystalline−amorphous BCPs,[28,29,31] epitaxially crystallized onto BA.

Further complexity for the BCPs may arise from the possible reciprocal heteroepitaxy of PE and iPP crystals.[42−45] As mentioned above, in binary blends of iPP and PE, epitaxial crystallization of PE on the oriented iPP substrate has been observed.[42−45] In this case, the $(100)_{PE}$ plane of PE and the $(010)_{iPP}$ plane of iPP are the contact planes,[42−45] and chain axis *c* of PE is aligned parallel to the [101] direction of iPP in the α form (the short diagonal of the *ac* face),[42−45] and, therefore, it is tilted to about 50° to the chain axis of iPP,[45] as shown in Figure 4C.

For our BCPs, this complexity results, however, in a simple final morphology. In fact, from the schemes of Figure 4A−C, note that if PE and iPP crystallize onto BA independently, a combination of the alignments of lamellae shown in Figure 4A,B will occur, with the c_{PE} axis of PE aligned parallel to the a_{BA} axis of BA (Figure 4B), which, in turn, is parallel to the $[101]_{iPP}$ direction of iPP (Figure 4A). This results at the end with an alignment of the c_{PE} axis of PE along the $[101]_{iPP}$ direction of iPP crystals and tilted to about 50° to the c_{iPP} axis of iPP, exactly as for the epitaxy of PE onto iPP crystals (Figure 4C). Therefore, eventual heteroepitaxy of PE and iPP gives the same alignment of PE and iPP lamellae as in the independent epitaxy of iPP and PE onto BA. This suggests that for iPP−PE/BA crystallization, iPP and PE can crystallize separately onto BA, and if upon cooling the melt iPP crystallizes first at higher temperature, PE may crystallize epitaxially either onto BA or iPP. The final alignment featured by a unique orientation of PE and a double orientation of iPP lamellae is the same. A scheme of the final orientations of iPP and PE lamellae onto BA is represented in Figure 4D, and the correlations between lattice parameters are

$$(010)_{iPP}//(001)_{BA}//(100)_{PE}$$

$$c_{PE}//a_{BA}//[101]_{iPP}$$

$$b_{PE}//b_{BA} \approx d(\bar{1}01)_{iPP}$$

The EDPs of Figure 3 and the relative alignments of iPP and PE lamellar crystals of Figure 4 confirm that in the morphologies of BCPs, as shown in Figure 2B−D, the thick lamellae highly oriented along one direction correspond to PE aligned with the *b* axis along the *b* axis of BA, and the thinner lamellae with a double orientation are the two families of iPP lamellae aligned with the chain axes nearly 60−70° apart and inclined to about ±50° to the c_{PE} axis of PE and to the a_{BA} axis of BA. In the regions of the BF-TEM images of Figure 2B−D showing the single lamellae orientation (delimited by the dashed lines), PE determines the morphology because it probably crystallizes before iPP. Therefore, iPP crystallizes after PE and its double alignment is not seen in these areas of the BF-TEM images because it is trapped between the oriented PE lamellae.[33] The iPP-trapped lamellae are probably parallel to the PE lamellae, but the chains of iPP in the trapped lamellae are tilted to the basal fold surface of the lamellae accounting for the EDPs and the double orientation. Analogously, in the regions of the BF-TEM images showing a double orientation of iPP lamellae, iPP crystallizes before PE and imposes the morphology. PE crystallizes after iPP between preformed iPP lamellae and it is probable that, in these regions, iPP and PE lamellae are parallel and chains of confined PE lamellae are inclined to the basal fold surface.[33]

It is worth mentioning that compared to the case of epitaxial crystallization of the two homopolymers,[39−41] the epitaxial crystallization of BCPs generates two types of domains that correspond to the crystallization of PE first or of iPP first with

https://dx.doi.org/10.1021/acs.macromol.0c01316
Macromolecules XXXX, XXX, XXX−XXX

the amorphous interlamellar material (iPP and PE, respectively) crystallizing in the confined interlamellar space. This confined crystallization should result in very different stabilities of the crystals formed.

The alignment of the PE crystals in the BCPs crystallized onto BA has been further confirmed by DF imaging of crystalline lamellae using the strong $(020)_{PE}$ reflection of PE, the most visible reflection in the EDPs of Figure 3B,C. DF imaging using a single diffraction spot should reveal only the PE crystals oriented in such a way to generate that reflection, and considering the hypothesized high single-crystal-like alignment of PE crystals, the entire set of PE lamellae should be revealed.

The EDP and the corresponding DF image produced with the $(020)_{PE}$ reflection of the sample iPP−PE-40 epitaxially crystallized onto BA are represented in Figure 5A,B,

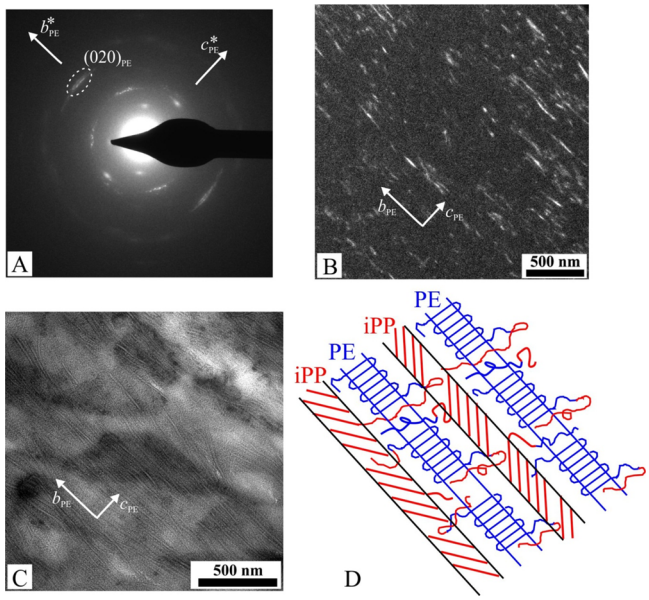

Figure 5. EDP (A), $(020)_{PE}$ DF (B), and BF-TEM (C) images of iPP−PE-40 epitaxially crystallized onto BA, and scheme of the revealed alignment of PE and iPP lamellae (D) defined by the EDP in A and DF image in B. DF (B) and BF (C) images are taken in the same area of the EDP in A. The alignment of b_{PE} and c_{PE} axes of PE is drawn. In the DF image the white strips represent the PE crystals in the diffraction condition that have generated the $(020)_{PE}$ reflection in the EDP. In the sketch D, the iPP lamellae are trapped between PE lamellae and the c_{iPP} axes of iPP are tilted to the basal fold surface and tilted to about 50° to the c_{PE} axis of PE, as pointed out by the EDP.

respectively. The BF image of the same film stained with RuO_4 in the same orientation as in the ED patter and dark-filed image is shown in Figure 5C. In the BF image, RuO_4 vapors stain the amorphous phases of PE and iPP that appear dark, whereas crystalline lamellae are the lighter strips aligned along one direction, presumably corresponding to the lamellae of PE (Figure 5C). The DF image of Figure 5B shows white elongated strips that corresponds to the PE crystals that have generated the $(020)_{PE}$ reflection, aligned along one direction. As suggested by the alignment of the EDP of Figure 5A, the revealed PE crystals are lamellae aligned along the b_{PE} axis direction of PE, that is, with the b_{PE} axis parallel to the b_{BA} axis of BA and the c_{PE} axis of PE aligned perpendicular to the white strips. The DF image, therefore, reveals the same parallel orientation of PE lamellae visualized in the BF image (Figure 5C), confirming that PE lamellae are aligned edge-on on the BA surface, with the b_{PE} axis of PE parallel to the b_{BA} axis of BA and the c_{PE} axis of PE parallel to the a_{BA} axis of BA, as schematically shown in Figure 4D. The dark regions in the DF image of Figure 5B are the amorphous phase and lamellar crystals of iPP trapped between PE lamellae, and also PE crystals in different orientations and, therefore, out of the diffraction conditions. A scheme of PE lamellae aligned as dictated by the EDP of Figure 5A and the DF image of Figure 5B, showing also the iPP lamellae, trapped between PE lamellae is represented in Figure 5D. Because the BF image of Figure 5C shows a unique lamellae orientation and the EDP of Figure 5A shows a double alignment of iPP, the morphology is defined by the unique alignment of PE lamellae, and the trapped iPP lamellae, as shown in Figure 5D, are parallel to PE but the c_{iPP} axes of iPP are tilted to the basal fold surface and tilted to about 50° to the c_{PE} axis of PE.

CONCLUSIONS

Crystalline−crystalline iPP−PE diblock copolymers composed of crystallizable iPP and PE blocks were prepared with a pyridylamidohafnium catalyst. Samples with different relative molecular masses of the iPP and PE blocks have been prepared. The microstructure of the iPP−PE BCPs has been studied in melt-crystallized samples, and correlations among phase separation, crystallization, and morphology have been investigated.

Phase-separated structures form at high temperatures in the melt because of the incompatibility between iPP and PE blocks. The microdomain structure has been revealed in samples rapidly crystallized by quenching the melt in liquid nitrogen. Cylindrical PE microdomains were seen for the copolymer iPP−PE-74 with a PE volume fraction of 26%. Small PE crystals are confined inside the PE cylindrical domains, while in the iPP matrix crystals of iPP are not visible because the quenching prevents crystallization of the lamellar α form and produces the formation of the mesomorphic form of iPP. Slow crystallization produces, instead, breakout crystallization, where the phase-separated structure produced in the melt is destroyed by the slow crystallization of the α form of iPP and of the orthorhombic for of PE.

BCP films have been epitaxially crystallized onto the surface of BA crystals to induce selective and different alignments of iPP and PE crystals. This allowed studying the succession of crystallization of iPP and PE and the resulting final morphology. The obtained morphology and the resulting orientation of crystalline iPP and PE phases have been analyzed by TEM in BF and DF modes and ED. Epitaxy produces oriented crystallization of PE and iPP, with a unique alignment of lamellae of PE and a double orientation of iPP lamellae onto the (001) exposed face of the BA substrate. The c_{PE} and b_{PE} axes of crystals of PE are aligned parallel to the a_{BA} and b_{BA} axes of the BA substrate, respectively. Two families of iPP lamellae of α form aligned along two different directions are also generated. The chain axes c_{iPP} of the two families of iPP lamellae are aligned parallel to the two edges of the $(010)_{iPP}$ plane of α form of iPP, precisely along two directions tilted 50° away from the crystallographic [101] direction of iPP, which is parallel to the a_{BA} axis of BA and, hence, parallel to the chain axis c_{PE} of PE. The two families of iPP lamellae are therefore nearly rotated 60−70° apart and inclined to about 50° to the c_{PE} axis of PE. The different alignments of PE and

https://dx.doi.org/10.1021/acs.macromol.0c01316
Macromolecules XXXX, XXX, XXX−XXX

iPP lamellae allowed to recognize the PE and iPP crystalline phases.

The epitaxial crystallization destroys the melt phase-separated structure but induces the formation of ordered lamellar nanostructures with alternated layers of iPP and PE whose orientation is defined by the alignment of PE or iPP crystalline phases, which in turn is determined by epitaxy. The definitive microstructure is different depending on whether PE crystallizes before iPP or *vice versa*. The epitaxial crystallization generated two types of domains that correspond to the crystallization of PE first or of iPP first with the amorphous interlamellar material (iPP and PE, respectively) crystallizing in the confined interlamellar space. The succession of crystallization determines the overall microstructure with unique or double orientation of nanodomains.

The results indicate that crystalline block copolymers offer the opportunity to create nanoscale patters on thin films and to improve the possibility of controlling the microstructure of BCPs and the alignment of microdomains through controlling the crystallization process.

■ ASSOCIATED CONTENT

Supporting Information

The Supporting Information is available free of charge at https://pubs.acs.org/doi/10.1021/acs.macromol.0c01316.

Additional BF TEM images of thin films of the BCPs crystallized from the melt without the BA substrate, details of the EDPs and comparison between the observed Bragg distances of the main *hkl* reflections observed in the EDPs of the iPP homopolymer and PE−iPP BCP thin films epitaxially crystallized onto BA, and the values of the literature Bragg distances (PDF)

■ AUTHOR INFORMATION

Corresponding Author

Claudio De Rosa − *Dipartimento di Scienze Chimiche, Università di Napoli Federico II, I-80126 Napoli, Italy;* orcid.org/0000-0002-5375-7475; Email: claudio.derosa@unina.it

Authors

Anna Malafronte − *Dipartimento di Scienze Chimiche, Università di Napoli Federico II, I-80126 Napoli, Italy;* orcid.org/0000-0002-7854-5823

Rocco Di Girolamo − *Dipartimento di Scienze Chimiche, Università di Napoli Federico II, I-80126 Napoli, Italy;* orcid.org/0000-0001-8815-2997

Finizia Auriemma − *Dipartimento di Scienze Chimiche, Università di Napoli Federico II, I-80126 Napoli, Italy;* orcid.org/0000-0003-4604-2057

Miriam Scoti − *Dipartimento di Scienze Chimiche, Università di Napoli Federico II, I-80126 Napoli, Italy;* orcid.org/0000-0001-9225-1509

Odda Ruiz de Ballesteros − *Dipartimento di Scienze Chimiche, Università di Napoli Federico II, I-80126 Napoli, Italy;* orcid.org/0000-0003-4940-421X

Geoffrey W. Coates − *Department of Chemistry and Chemical Biology, Baker Laboratory, Cornell University, Ithaca, New York 14853-1301, United States;* orcid.org/0000-0002-3400-2552

Complete contact information is available at: https://pubs.acs.org/10.1021/acs.macromol.0c01316

Notes

The authors declare no competing financial interest.

■ ACKNOWLEDGMENTS

The task force "Polymers and biopolymers" of the University of Napoli Federico II is acknowledged. This research was supported by the Center for Sustainable Polymers, a National Science Foundation (NSF) Center for Chemical Innovation (CHE-1901635) and Cornell University.

■ REFERENCES

(1) Eagan, J. M.; Xu, J.; Di Girolamo, R.; Thurber, C. M.; Macosko, C. W.; LaPointe, A. M.; Bates, F. S.; Coates, G. W. Combining polyethylene and polypropylene: Enhanced performance with PE/iPP multiblock polymers. *Science* **2017**, *355*, 814.

(2) Xu, J.; Eagan, J. M.; Kim, S.-S.; Pan, S.; Lee, B.; Klimovica, K.; Jin, K.; Lin, T.-W.; Howard, M. J.; Ellison, C. J.; LaPointe, A. M.; Coates, G. W.; Bates, F. S. Compatibilization of Isotactic Polypropylene (iPP) and High-Density Polyethylene (HDPE) with iPP-PE Multiblock Copolymers. *Macromolecules* **2018**, *51*, 8585.

(3) Shan, C. L. P.; Walton, K. L.; Marchand, G. R.; Carnahan, E. M.; Karjala, T. Crystalline block composites as compatibilizers. U.S. Patent 8,822,599 B2, 2014.

(4) Geyer, R.; Jambeck, J. R.; Law, K. L. Production, use, and fate of all plastics ever made. *Sci. Adv.* **2017**, *3*, No. e1700782.

(5) Malpass, D. B.; Band, E. I. *Introduction to Industrial Polypropylene: Properties, Catalysis, Processes*; Scrivener, Wiley, 2012.

(6) Busico, V.; Cipullo, R.; Friederichs, N.; Ronca, S.; Togrou, M. The First Molecularly Characterized Isotactic Polypropylene-Block-Polyethylene Obtained Via "Quasi-Living" Insertion Polymerization. *Macromolecules* **2003**, *36*, 3806.

(7) Domski, G. J.; Rose, J. M.; Coates, G. W.; Bolig, A. D.; Brookhart, M. Living Alkene Polymerization: New Methods for the Precision Synthesis of Polyolefins. *Prog. Polym. Sci.* **2007**, *32*, 30.

(8) Coates, G. W.; Hustad, P. D.; Reinartz, S. Catalysts for the Living Insertion Polymerization of Alkenes: Access to New Polyolefin Architectures Using Ziegler-Natta Chemistry. *Angew. Chem., Int. Ed.* **2002**, *41*, 2236.

(9) Domski, G. J.; Eagan, J. M.; De Rosa, C.; Di Girolamo, R.; LaPointe, A. M.; Lobkovsky, E. B.; Talarico, G.; Coates, G. W. Combined Experimental and Theoretical Approach for Living and Isoselective Propylene Polymerization. *ACS Catal.* **2017**, *7*, 6930.

(10) Coates, G. W.; Domski, G. J. Pyridylamidohafnium catalyst precursors, active species from this and uses thereof to polymerize alkenes. Patent WO 2008112133 A2, 2008.

(11) Domski, G. J.; Edson, J. B.; Keresztes, I.; Lobkovsky, E. B.; Coates, G. W. Synthesis of a new olefin polymerization catalyst supported by an sp^3-C donor via insertion of a ligand-appended alkene into the Hf−C bond of a neutral pyridylamidohafnium trimethyl complex. *Chem. Commun.* **2008**, 6137.

(12) Domski, G. J.; Lobkovsky, E. B.; Coates, G. W. Polymerization of α-Olefins with Pyridylamidohafnium Catalysts: Living Behavior and Unexpected Isoselectivity from a C_s-Symmetric Catalyst Precursor. *Macromolecules* **2007**, *40*, 3510.

(13) Castillo, R. V.; Müller, A. J. Crystallization and morphology of biodegradable or biostable single and double crystalline block copolymers. *Prog. Polym. Sci.* **2009**, *34*, 516.

(14) Hamley, I. W. Crystallization on Block Copolymers. *Adv. Polym. Sci.* **1999**, *148*, 113.

(15) Loo, Y. L.; Register, R. A. Crystallization Within Block Copolymer Mesophases. In *Development in Block Copolymer Science and Technology*; Hamley, I. W., Ed.; John Wiley & Sons, Ltd.: Chichester, 2004; p 213.

(16) Müller, A. J.; Balsamo, V.; Arnal, M. L. Nucleation and crystallization in diblock and triblock copolymers. *Adv. Polym. Sci.* **2005**, *190*, 1.

(17) Hamley, I. W. *The Physics of Block Copolymers*; Oxford University Press: Oxford, 1998.

https://dx.doi.org/10.1021/acs.macromol.0c01316
Macromolecules XXXX, XXX, XXX−XXX

(18) Bates, F. S.; Fredrickson, G. H. Block Copolymer Thermodynamics: Theory and Experiment. *Annu. Rev. Phys. Chem.* **1990**, *41*, 525.
(19) Whitesides, G.; Mathias, J.; Seto, C. Molecular self-assembly and nanochemistry: a chemical strategy for the synthesis of nanostructures. *Science* **1991**, *254*, 1312.
(20) Thurn-Albrecht, T.; Schotter, J.; Kastle, G. A.; Emley, N.; Shibauchi, T.; Krusin-Elbaum, L.; Guarini, K.; Black, C. T.; Tuominen, M. T.; Russell, T. P. Ultrahigh-density nanowire arrays grown in self-assembled diblock copolymer templates. *Science* **2000**, *290*, 2126.
(21) Park, M.; Harrison, C. K.; Chaikin, P. M.; Register, R. A.; Adamson, D. H. Block Copolymer Lithography: Periodic Arrays of $\sim 10^{11}$ Holes in 1 Square Centimeter. *Science* **1997**, *276*, 1401.
(22) Park, C.; Yoon, J.; Thomas, E. L. Enabling nanotechnology with self assembled block copolymer patterns. *Polymer* **2003**, *44*, 6725.
(23) De Rosa, C.; Auriemma, F.; Di Girolamo, R.; Pepe, G. P.; Napolitano, T.; Scaldaferri, R. Enabling Strategies in Organic Electronics Using Ordered Block Copolymer Nanostructures. *Adv. Mater.* **2010**, *22*, 5414.
(24) De Rosa, C.; Auriemma, F.; Diletto, C.; Di Girolamo, R.; Malafronte, A.; Morvillo, P.; Zito, G.; Rusciano, G.; Pesce, G.; Sasso, A. Toward hyperuniform disordered plasmonic nanostructures for reproducible surface-enhanced Raman spectroscopy. *Phys. Chem. Chem. Phys.* **2015**, *17*, 8061.
(25) Auriemma, F.; De Rosa, C.; Malafronte, A.; Di Girolamo, R.; Santillo, C.; Gerelli, Y.; Fragneto, G.; Barker, R.; Pavone, V.; Maglio, O.; Lombardi, A. A Nano-In-Nano Approach for Enzyme Immobilization Based on Block Copolymers. *ACS Appl. Mater. Interfaces* **2017**, *9*, 29318.
(26) Loo, Y.-L.; Register, R. A.; Ryan, A. J. Modes of Crystallization in Block Copolymer Microdomains: Breakout, Templated, and Confined. *Macromolecules* **2002**, *35*, 2365.
(27) Lee, L.-B. W.; Register, R. A. Equilibrium Control of Crystal Thickness and Melting Point through Block Copolymerization. *Macromolecules* **2004**, *37*, 7278.
(28) De Rosa, C.; Park, C.; Thomas, E. L.; Lotz, B. Microdomain patterns via directional eutectic solidification and epitaxy. *Nature* **2000**, *405*, 433.
(29) De Rosa, C.; Park, C.; Lotz, B.; Wittmann, J.-C.; Fetters, L. J.; Thomas, E. L. Control of Molecular and Microdomain Orientation in a Semicrystalline Block Copolymer Thin Film by Epitaxy. *Macromolecules* **2000**, *33*, 4871.
(30) Park, C.; De Rosa, C.; Fetters, L. J.; Lotz, B.; Thomas, E. L. Alteration of Classical Microdomain Patterns of Block Copolymers by Degenerate Epitaxy. *Adv. Mater.* **2001**, *13*, 724.
(31) Park, C.; Di Rosa, C.; Lotz, B.; Fetters, L. J.; Thomas, E. L. Molecular and Microdomain Orientation in Semicrystalline Block Copolymer Thin Films by Directional Crystallization of the Solvent and Epitaxy. *Macromol. Chem. Phys.* **2003**, *204*, 1514.
(32) De Rosa, C.; Auriemma, F.; Di Girolamo, R.; Aprea, R.; Thierry, A. Selective Gold Deposition on a Nanostructured Block Copolymer Film Crystallized by Epitaxy. *Nano Res.* **2011**, *4*, 241.
(33) De Rosa, C.; Di Girolamo, R.; Auriemma, F.; D'Avino, M.; Talarico, G.; Cioce, C.; Scoti, M.; Coates, G. W.; Lotz, B. Oriented Microstructures of Crystalline-Crystalline Block Copolymers Induced by Epitaxy and Competitive and Confined Crystallization. *Macromolecules* **2016**, *49*, 5576.
(34) De Rosa, C.; Di Girolamo, R.; Auriemma, F.; Talarico, G.; Malafronte, A.; Scarica, C.; Scoti, M. Controlling Size and Orientation of Lamellar Microdomains in Crystalline Block Copolymers. *ACS Appl. Mater. Interfaces* **2017**, *9*, 31252.
(35) De Rosa, C.; Di Girolamo, R.; Malafronte, A.; Scoti, M.; Talarico, G.; Auriemma, F.; Ruiz de Ballesteros, O. Polyolefins based crystalline block copolymers: ordered nanostructures from control of crystallization. *Polymer* **2020**, *196*, 122423.
(36) Wittmann, J. C.; Lotz, B. Epitaxial Crystallization of Polymers on Organic and Polymeric Substrates. *Prog. Polym. Sci.* **1990**, *15*, 909.
(37) Wittmann, J. C.; Lotz, B. Epitaxial Crystallization of Polyethylene on Organic Substrates: A Reappraisal of the Mode of Action of Selected Nucleating Agents. *J. Polym. Sci., Polym. Phys. Ed.* **1981**, *19*, 1837.
(38) Wittmann, J. C.; Lotz, B. Epitaxial Crystallization of Monoclinic and Orthorhombic Polyethylene Phases. *Polymer* **1989**, *30*, 27.
(39) Wittmann, J. C.; Hodge, A. M.; Lotz, B. Epitaxial Crystallization of Polymers Onto Benzoic Acid: Polyethylene and Paraffins, Aliphatic Polyesters, and Polyamides. *J. Polym. Sci., Polym. Phys. Ed.* **1983**, *21*, 2495.
(40) Mathieu, C.; Thierry, A.; Wittmann, J. C.; Lotz, B. "Multiple" nucleation of the (010) contact face of isotactic polypropylene, α phase. *Polymer* **2000**, *41*, 7241.
(41) Stocker, W.; Magonov, S. N.; Cantow, H. J.; Wittmann, J. C.; Lotz, B. Contact Faces of Epitaxially Crystallized α- and γ-Phase Isotactic Polypropylene Observed by Atomic Force Microscopy. *Macromolecules* **1993**, *26*, 5915.
(42) Gross, B.; Peterman, J. Synergisms of mechanical properties in blends of semi-crystalline polymers. *J. Mater. Sci.* **1984**, *19*, 105.
(43) Yan, S.; Yang, D.; Petermann, J. Controlling factors for the occurrence of heteroepitaxy of polyethylene on highly oriented isotactic polypropylene. *Polymer* **1998**, *39*, 4569.
(44) Li, H.; Yan, S. Surface-Induced Polymer Crystallization and the Resultant Structures and Morphologies. *Macromolecules* **2011**, *44*, 417.
(45) Lotz, B.; Wittmann, J. C. Polyethylene-Isotactic Polypropylene Epitaxy: Analysis of the Diffraction Patterns of Oriented Biphasic Blends. *J. Polym. Sci., Part B: Polym. Phys.* **1987**, *25*, 1079.
(46) Bassett, G. A. New Technique for Decoration of Cleavage and Slip Steps on Ionic Crystal Surfaces. *Philos. Mag.* **1958**, *3*, 1042.
(47) Wittmann, J. C.; Lotz, B. Polymer Decoration: The Orientation of Polymer Folds as Revealed by The Crystallisation of Polymer Vapors. *J. Polym. Sci., Polym. Phys. Ed.* **1985**, *23*, 205.
(48) Ayache, J.; Beaunier, L.; Boumendil, J.; Ehret, G.; Laub, D. *Sample Preparation Handbook for Transmission Electron Microscopy Techniques*; Springer: New York, 2010; Chapter 7, p 279.
(49) Zia, Q.; Androsch, R.; Radusch, H.-J.; Piccarolo, S. Morphology, reorganization and stability of mesomorphic nanocrystals in isotactic polypropylene. *Polymer* **2006**, *47*, 8163.
(50) Zia, Q.; Androsch, R.; Radusch, H.-J.; Ingoliç, E. Crystal morphology of rapidly cooled isotactic polypropylene: A comparative study by TEM and AFM. *Polym. Bull.* **2008**, *60*, 791.
(51) De Rosa, C.; Auriemma, F.; Di Girolamo, R.; Ruiz de Ballesteros, O.; Pepe, M.; Tarallo, O.; Malafronte, A. Morphology and Mechanical Properties of the Mesomorphic Form of Isotactic Polypropylene in Stereodefective Polypropylene. *Macromolecules* **2013**, *46*, 5202.
(52) De Rosa, C.; Auriemma, F.; Tarallo, O.; Malafronte, A.; Di Girolamo, R.; Esposito, S.; Piemontesi, F.; Liguori, D.; Morini, G. The "Nodular" α Form of Isotactic Polypropylene: Stiff and Strong Polypropylene with High Deformability. *Macromolecules* **2017**, *50*, 5434.
(53) Bruno, G.; Randaccio, L. Refinement of the Benzoic Acid Structure at Room Temperature. *Acta Crystallogr., Sect. B: Struct. Crystallogr. Cryst. Chem.* **1980**, *36*, 1711.
(54) Bunn, C. W. The crystal structure of long-chain normal paraffin hydrocarbons. The "shape" of the CH_2 group. *Trans. Faraday Soc.* **1939**, *35*, 482.
(55) Natta, G.; Corradini, P. Structure and Properties of Isotactic Polypropylene. *Nuovo Cimento, Suppl.* **1960**, *15*, 40.
(56) Auriemma, F.; De Rosa, C.; Malafronte, A.; Scoti, M.; Di Girolamo, R. Solid State Polymorphism of Isotactic and Syndiotactic Polypropylene. In *Polypropylene Handbook*; Karger-Kocsis, J., Bárány, T., Eds.; Springer: Cham, 2019.
(57) Lotz, B.; Wittmann, J. C. The Molecular Origin of Lamellar Branching in the α (Monoclinic) Form of Isotactic Polypropylene. *J. Polym. Sci., Part B: Polym. Phys.* **1986**, *24*, 1541.
(58) Padden, F. J., Jr.; Keith, H. D. Crystallization in Thin Films of Isotactic Polypropylene. *J. Appl. Phys.* **1966**, *37*, 4013.

https://dx.doi.org/10.1021/acs.macromol.0c01316
Macromolecules XXXX, XXX, XXX−XXX

(59) Khoury, F. The Spherulitic Crystallization of Isotactic Polypropylene From Solution: On the Evolution of Monoclinic Spherulites From Dendritic Chain-Folded Crystal Precursors. *J. Res. Natl. Bur. Stand., Sect. A* **1966**, *70*, 29.
(60) Lotz, B.; Graff, S.; Wittmann, J. C. Crystal Morphology of the γ (Triclinic) Phase of Isotactic Polypropylene and its Relation to the α Phase. *J. Polym. Sci., Polym. Phys.* **1986**, *24*, 2017.
(61) Meille, S. V.; Brückner, S. Non-parallel chains in crystalline γ-isotactic polypropylene. *Nature* **1989**, *340*, 455.
(62) Meille, S. V.; Bruckner, S.; Porzio, W. γ-Isotactic Polypropylene. A Structure with Nonparallel Chain Axes. *Macromolecules* **1990**, *23*, 4114.
(63) Hikosaka, M.; Seto, T. The Order of the Molecular Chains in Isotactic Polypropylene Crystals. *Polym. J.* **1973**, *5*, 111.

https://dx.doi.org/10.1021/acs.macromol.0c01316
Macromolecules XXXX, XXX, XXX−XXX